

UC Berkeley

UC Berkeley Previously Published Works

Title

Marine sulphate captures a Paleozoic transition to a modern terrestrial weathering environment.

Permalink

<https://escholarship.org/uc/item/3sz798q0>

Journal

Nature Communications, 16(1)

Authors

Waldeck, Anna

Olson, Haley

Crockford, Peter

et al.

Publication Date

2025-03-01

DOI

10.1038/s41467-025-57282-y

Peer reviewed

Marine sulphate captures a Paleozoic transition to a modern terrestrial weathering environment

Received: 18 July 2024

Accepted: 18 February 2025

Published online: 01 March 2025

 Check for updates

Anna R. Waldeck ^{1,10,11} , Haley C. Olson ^{1,11} , Peter W. Crockford ^{1,2,3}, Abby M. Couture⁴, Benjamin R. Cowie¹, Eben B. Hodgin ^{1,5}, Kristin D. Bergmann ⁶, Keith Dewing ⁷, Stephen E. Grasby ⁷, Ryan J. Clark ⁸, Francis A. Macdonald ^{1,9} & David T. Johnston ¹ 

The triple oxygen isotope composition of sulphate minerals has been used to constrain the evolution of Earth's surface environment (e.g., pO_2 , pCO_2 and gross primary productivity) throughout the Proterozoic Eon. This approach presumes the incorporation of atmospheric O_2 atoms into riverine sulphate via the oxidative weathering of pyrite. However, this is not borne out in recent geological or modern sulphate records, where an atmospheric signal is imperceptible and where terrestrial pyrite weathering occurs predominantly in bedrock fractures that are physically more removed from atmospheric O_2 . To better define the transition from a Proterozoic to a modern-like weathering regime, here we present new measurements from twelve marine evaporite basins spanning the Phanerozoic. These data display a step-like transition in the triple oxygen isotope composition of evaporite sulphate during the mid-Paleozoic (420 to 387.7 million years ago). We propose that the evolution of early root systems deepened the locus of pyrite oxidation and reduced the incorporation of O_2 into sulphate. Further, the early Devonian proliferation of land plants increased terrestrial organic carbon burial, releasing free oxygen that fueled increased redox recycling of soil-bound iron and resulted in the final rise in pO_2 to modern-like levels.

The central targets for reconstructing Earth's ancient atmosphere and climate are pCO_2 and pO_2 as they intimately relate to Earth's habitability and global metabolism¹. Traditionally, paleo-atmospheric composition is indirectly inferred via stable isotope reconstructions^{2–4} or through the directionality of change in redox sensitive metals and their isotopes in marine sediments^{5–7}. As the

diversity of approaches to constrain atmospheric chemistry has increased, so too has our uncertainty of the timing of Earth's rise to modern-like pO_2 levels. These estimates span over 500 million years, a wider range than constraints on the original Great Oxidation Event ca. 2500–2200 Ma^{8–13}. This uncertainty in timing has prevented the isolation of the mechanism(s) that drove oxygenation (e.g., tectonics,

¹Department of Earth and Planetary Sciences, Harvard University, Cambridge, MA, USA. ²Woods Hole Oceanographic Institution, Woods Hole, MA, USA.

³Department of Earth Sciences, Carleton University, Ottawa, ON, Canada. ⁴Department of Geosciences, Wellesley College, Wellesley, MA, USA. ⁵Department of Earth, Environmental and Planetary Sciences, Brown University, Providence, RI, USA. ⁶Department of Earth, Atmospheric and Planetary Sciences, Massachusetts Institute of Technology, Cambridge, MA, USA. ⁷Natural Resources Canada, Geological Survey of Canada, Calgary, AB, Canada. ⁸Iowa Geological Survey, University of Iowa, Iowa City, IA, USA. ⁹Department of Earth and Planetary Science, University of California, Berkeley, Berkeley, CA, USA. ¹⁰Present address: Department of Geosciences, Pennsylvania State University, University Park, PA, USA. ¹¹These authors contributed equally: Anna R. Waldeck, Haley C. Olson.  e-mail: a.waldeck@psu.edu; haleyolson@g.harvard.edu; johnston@eps.harvard.edu

glaciation, or marine/terrestrial biology) and its ensuing redox implications, both of which are central to our understanding of the Earth system.

A more direct and emerging approach employing the triple oxygen isotope composition ($\Delta^{17}\text{O}$) of sulphate minerals was recently proposed as a sharper quantitative tool for ancient atmospheric reconstructions¹⁴. It is known from observations in the modern atmosphere that tropospheric O_2 carries a large, anomalous, and negative $\Delta^{17}\text{O}$ signature¹⁵. The magnitude of the isotope signature in atmospheric O_2 scales with pO_2 , pCO_2 , and gross primary production (GPP) as a result of atmospheric chemistry and overall isotope mass-balance¹⁵. It is well-documented in the Proterozoic (2500–539 Ma^{14,16,17}) that sulphate minerals carry a large, anomalously negative $\Delta^{17}\text{O}$ composition that is most likely derived from contemporaneous tropospheric O_2 . Existing Ediacaran measurements are difficult to assign to a marine evaporite basin since samples are from salt-plugs and nodular sulphates from Russia, which may have complex (non-marine) histories. The closest, unequivocally marine evaporites are found in Northwestern Canada and Victoria Island 820–750 Ma¹⁸ and refs. therein). Unlike Proterozoic sulphate records, the $\Delta^{17}\text{O}$ of Cretaceous–Cenozoic marine barite (BaSO_4)¹⁹, as well as studies of modern seawater²⁰ and riverine^{21–23} sulphate, show no resolvable atmospheric O_2 fingerprint. These geological sulphate catalogues instead record biogeochemistry – specifically, microbial sulphate reduction (MSR)^{19,20,22,24}. Today, it is thought that MSR partially resets the oxygen isotope composition of marine sulphate to an isotopic equilibrium with environmental H_2O ^{19,20,23,25}, and further that terrestrial pyrite oxidation (and sulphate generation) does not adopt a resolvable atmospheric signal²². At face value then, Earth's sulphur and oxygen cycles must have changed significantly sometime between ~800–130 Ma to preclude the incorporation of atmospheric O_2 signatures into marine sulphate.

Generally, during pyrite oxidation, Fe^{3+} (and to a lesser extent, O_2) steals electrons from pyrite to generate aqueous sulphate and Fe^{2+} ^{26,27}. The rate of this reaction is largely a function of oxidant availability, which in turn is related to diffusion and transport of electron acceptors to the pyrite surface²⁸. Numerous (labeled and unlabeled) isotope studies have tried to constrain the sources of oxygen atoms in the sulphate produced from pyrite oxidation over a range of temperature, pressure, pH and (a)biological conditions (see SI section 5). With heterogeneous results, these experiments commonly observe that sulphate obtains 0–30% of its O atoms from O_2 , with the remaining O atoms donated from H_2O ^{29–36}. At a more granular level, the capacity to directly incorporate an O atom from O_2 into sulphate is a function of the local availability of Fe^{3+} ³⁰, whereby elevated iron contents and vigorous iron redox recycling limits the direct incorporation of O_2 into sulphate. This leaves an obvious role for iron cycling in affecting the isotopic composition of sulphate across Earth history.

Results and Discussion

Here we present 189 new high-precision³⁷ triple oxygen isotope ($\delta^{18}\text{O}$, $\Delta^{17}\text{O}$) measurements from twelve heavily sampled, globally distributed and volumetrically significant marine sulphate evaporite basins spanning the last 542 million years of Earth history (Fig. 1, Supplementary Data 1, and Tables S2 & S3 for more information). We treat each evaporite basin, sampled with between 5 and 49 measurements, as representative of marine sulphate at the time of deposition. This is supported by the fact that the contemporaneous basins yield statistically indistinguishable oxygen isotope compositions (e.g., Canadian Prairie Formation and the Iowa Pinicon Ridge Formation, see Table S3). Each basin carries some internal variability in both $\delta^{18}\text{O}$ and $\Delta^{17}\text{O}$ associated with basin restriction, depositional timescales, and secondary processes (see²⁴ and SI for calibration, correction factors, and extended statistical analyses). However, the most significant feature of the data set is a step change in $\Delta^{17}\text{O}$ in the

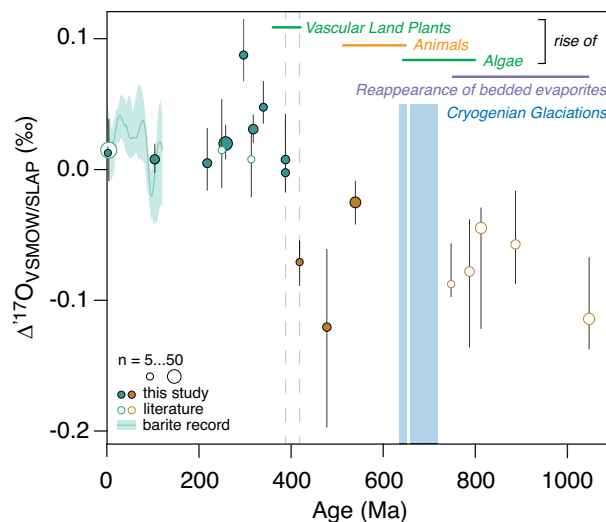


Fig. 1 | A billion-year record of the oxygen isotope composition of marine sulphate. The oxygen isotope composition ($\Delta^{17}\text{O}$) of volumetrically significant marine sulphate evaporite basins over approximately the last 1050 million years. Filled (this study) and open circles (published data^{16,18,24} scaled, see SI) are represented as a function of samples per basin, centered on the median value, and with error bars that denote the 25th and 75th quartiles of each distribution. A smoothed fit, with a 95% confidence interval for the Cenozoic–Cretaceous sulphate record is noted in the filled blue-green region¹⁹. At the top is a timeline of geologic events that have been linked to a rise in atmospheric pO_2 . The two Neoproterozoic Snowball Earth events (Cryogenian Glaciations) are represented by vertical blue bars. Data from Marinoan barite crystal fans¹⁶ (i.e., not evaporite deposits) is excluded. The gray dashed bars represent the temporal constraint on pO_2 rise based on the marine sulphate evaporite record.

mid-Paleozoic, supported by a Wilcoxon rank sum test ($p < 0.05$). The basins ≤ 387.7 Ma ($n = 9$ with this study, $n = 3$ from scaled published data^{16,24}, see SI) are overlapping in both $\Delta^{17}\text{O}$ and $\delta^{18}\text{O}$ (with inter-quartile ranges of 0.2 to 3.3‰ for $\delta^{18}\text{O}$ and 0.01 to 0.06‰ for $\Delta^{17}\text{O}$), carry near-zero $\Delta^{17}\text{O}$ compositions and overall lower $\delta^{18}\text{O}$ values (see Table S2, Fig. 2). Conversely, eight basins between 1050 and 420 Ma ($n = 3$ with this study, $n = 5$ from scaled published data¹⁸) have overall higher and more variable $\delta^{18}\text{O}$ and significantly more negative $\Delta^{17}\text{O}$ compositions (see Table S2, Fig. 2). A two-sample t-test finds that the younger (≤ 387.7 Ma) and older (≥ 420 Ma) $\Delta^{17}\text{O}$ populations are distinct and statistically offset by between 0.08 and 0.10‰ (as defined by the 95% confidence interval). These two populations of data capture a state change in the composition of marine sulphate, which requires a transition in the interaction of the sulphur and oxygen cycles between 420 and 387.7 Ma.

Possible Drivers of Sulphate Oxygen Isotope Change

The timing of the transition in the $\Delta^{17}\text{O}$ composition of marine sulphate is later than most events thought to drive significant changes in atmospheric pO_2 . These events include the Neoproterozoic Snowball Earth glaciations^{16,38}, the origin of animals³⁹, the onset of vigorous marine bioturbation^{40,41}, inferred changes in Ediacaran ocean redox conditions³⁹, and the initial deposition of large, bedded evaporite deposits⁴². All of these events, separated by >300 million years, have been argued to be drivers or products of changes to the inventory of atmospheric O_2 . However, given that marine evaporites formed between 420 Ma and 1050 Ma are isotopically consistent and distinct from younger units, it is now apparent that none of these triggers or events ushered in a change in O_2 significant enough to be resolved in the $\Delta^{17}\text{O}$ sulphate record. Instead, the loss of negative, anomalous $\Delta^{17}\text{O}$ signatures coincides with the proliferation of vascular land plants and coincident change in terrestrial soils^{43,44}. The question then

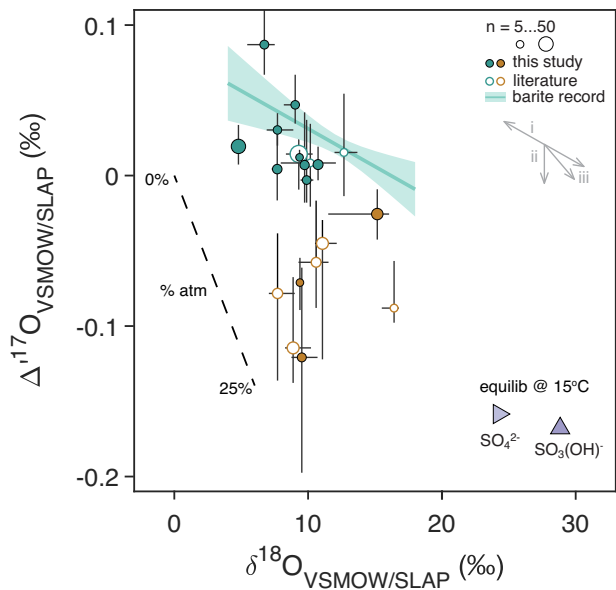


Fig. 2 | Triple oxygen isotope composition of marine sulphate minerals. The triple oxygen isotope composition ($\Delta^{17}\text{O}$ against $\delta^{18}\text{O}$) of marine sulphate evaporite deposits (filled circles=this work; open circles=literature^{16,18,24}; marker size scales with sample set size). Each circle reflects the median basinal value, with error bars reflecting the 25th and 75th percentiles. As in Fig. 1, blue-green symbols reflect basins ≤ 387.7 Ma, whereas brown symbols are ≥ 420 Ma. The light blue-green regression line reflects the Cenozoic-Cretaceous marine barite record¹⁹. The two triangles in the lower right are sulphate isomer equilibrium with seawater at 15 °C²³. The long-dashed line – approximated as linear – represents sulphate that derives between 0 to 25% of its O atoms from (modern) atmospheric O_2 and the remainder from seawater H_2O . Finally, a suite of vectors below the key indicates the directionality of change if (i) meteoric waters are involved, (ii) if paleo- O_2 had a more depleted $\Delta^{17}\text{O}$ composition, or (iii) if sulphate is overprinted via thermodynamic equilibria with seawater.

becomes – how did Earth’s major geochemical cycles (notably O and S) respond to this paleobiological innovation?

Since the Great Oxidation Event^{45,46}, tropospheric O_2 would have been the most significant carrier of a negative $\Delta^{17}\text{O}$ anomaly^{15,47}. As such, the negative $\Delta^{17}\text{O}$ preserved in sulphate deposits ≥ 420 Ma almost certainly preserves some fraction of contemporaneous atmospheric O_2 (Figure S7). The loss of the $\Delta^{17}\text{O}$ anomaly between 420 and 387.7 Ma requires either a change in sulphate generation pathways to preclude the entrainment of oxygen from O_2 , or a more vigorous S cycle capable of erasing a terrestrial O isotope anomaly via enhanced riverine or marine microbial sulphate recycling²⁰. Fortunately, the rich sedimentary record of $\delta^{34}\text{S}$ of pyrite helps inform this question. A statistical analysis of compiled $\delta^{34}\text{S}$ data illustrate that the mean offset between sulphate and sulphide is statistically identical from 500–300 Ma^{40,48}. Any significant change in MSR activity and a change in the relative importance of pyrite burial would manifest in the $\delta^{34}\text{S}$ record, suggesting that the more likely trigger in the $\Delta^{17}\text{O}$ signal is from terrestrial environments and pyrite oxidation itself.

A Transition in Pyrite Weathering

In the modern, rooted vascular plants deepen the locus of terrestrial pyrite weathering, physically and chemically breaking down substrates, and stabilizing a meter(s)-thick soil mantle⁴⁹. Beneath the soil layer, pyrite weathering reactions proceed within bedrock fractures²⁸. This environment is, in most cases, physically dislocated from contact with atmospheric O_2 , leaving diffusion responsible for the addition and subtraction of reactants and products at the literal site of pyrite oxidation²⁸. Diffused O_2 directly or indirectly catalyzes complex Fe–S–O redox cycling, with Fe^{3+} , S intermediates, and oxygen species

all serving as potential oxidants for pyrite. The consequence of the suite of oxidants in these environments is no resolvable isotopic relationship to modern atmospheric O_2 ^{22,23}. This is consistent with modern river systems, which are dominated by sulphate oxygen isotope compositions most easily explained via isotopic equilibrium with local waters²².

Similar to modern rivers and Cenozoic–Cretaceous barite^{19,22}, the ≤ 387.7 Ma marine evaporite record preserves a signal more related to equilibrium with water and MSR (see annotations on Fig. 2) than the addition of tropospheric O_2 . This suggests that a modern-like weathering regime was active in the early Devonian, making modern river systems, for example, a suitable proxy for the last 387.7 million years; the lack of mass-independent $\Delta^{17}\text{O}$ in sulphate is thus the expectation. In the early Paleozoic and throughout the Proterozoic, however, the isotope compositions of sulphate evaporites fall more toward vectors describing atmospheric O_2 incorporation (Fig. 2, dashed line; Figure S7). Excluded from the present discussion are the post-Marinoan glaciation barite crystal fans that record large, anomalous oxygen isotope depletions¹⁶. Although sulphate minerals, the barite crystal fans are not fit for direct comparison to evaporite records, being sedimentologically distinct, yet their interpretation may benefit from many of the arguments herein. In a world before soils, the locus of terrestrial pyrite oxidation would be shallower in the regolith⁴³, if not also drier⁴. These features would limit the capacity of Fe recycling to physically keep O_2 at a distance from pyrite and, as such, allow the incorporation of atmospheric O_2 . This is all in keeping with increasing water-rock interactions⁵⁰ and the generation of thick soils with secondary mineral phases in plant-influenced environments⁵¹. It also aligns with the experimental data that show, under some specific conditions, pyrite oxidation can indeed incorporate oxygen atoms from O_2 ^{30,32,52}.

Rise in Atmospheric Oxygen Fueled by Land Plants

The entire infrastructure on which the $\Delta^{17}\text{O}$ proxy is predicted ties the magnitude of the $\Delta^{17}\text{O}$ anomaly in sulphate to pCO_2 , pO_2 , and GPP. The fraction of sulphate oxygen derived from atmospheric O_2 is largely assumed to be invariant and often fixed at a range of 8–15%. Previous forward⁵³ and inverse^{3,54} models of Paleozoic atmospheric change vary widely, but most call on a dramatic mid-Paleozoic increase in pO_2/pCO_2 even before considering changes in GPP related to land plants (see SI for sensitivity tests, model outputs/predictions and expanded discussion). This modeled increase in pO_2/pCO_2 drives a predicted increase in the sulphate $\Delta^{17}\text{O}$, similar in direction to the observed evaporite record (Fig. 1). That said, if changes in pO_2 contributed to increased $\Delta^{17}\text{O}$, that oxygenation event would have to occur in the early Devonian. Instead, we propose that slowing or even stopping the capacity to incorporate O_2 into sulphate—making the fraction of O from O_2 negligible—is a simpler and better fit to the data. If correct, the early Devonian may mark the end of the capacity of marine evaporites to record paleo-atmospheric compositions.

The energy required for oxidative weathering is ultimately linked to the atmospheric overburden of pO_2 . This requires enough molecular oxygen present by 420–387.7 Ma to power modern-like pyrite oxidation. This interval, the latest Silurian to Early Devonian, also captures the development of “true roots” in vascular land plants (e.g., ~407 Ma Rhynie Chert Lagerstätten) and generally deeper rooting systems—up to 1 m in depth^{44,55}. We hypothesize that the coincident shift in the $\Delta^{17}\text{O}$ composition of evaporites reflects a deepening of the global terrestrial weathering environment associated with these early rooting systems by at least 387.7 Ma. This argument supports the hypothesis that the proliferation of land plants took Earth to a modern-like S cycle with putatively modern-like levels of pO_2 ^{3,56}, perhaps through the increase in the C:P ratio of terrestrial biomass (e.g.⁵⁷), and enhanced terrestrial organic carbon burial associated with the Devonian proliferation of vascular plants. It also follows that the pO_2 levels

necessary to trigger the change in the $\Delta^{17}\text{O}$ signal were not crossed in the Neoproterozoic or early Paleozoic, as those evaporite $\Delta^{17}\text{O}$ signatures look more like the Proterozoic than Mesozoic–Cenozoic (see Figure S7). These findings allow for the refinement of models targeting the relationship between land plant evolution, GPP and atmospheric pO_2 (3, see SI for model simulations).

As marine sulphate stands as the largest oxidant pool in the modern ocean, its associated evaporite record provides a critical window into Earth's evolving redox budget. In reconstructing the last -1000 million years of seawater sulphate, the mid-Paleozoic holds a key transition—one from a world where atmospheric oxygen was commonly found in marine sulphate to an environment recording only mass-dependent biogeochemical cycling. This transition is coincident with the development of thicker terrestrial soils and the advent of rooted vascular plants. These changes would have driven pyrite oxidation deep into waterlogged environments, where a complex oxygen-driven Fe–S redox cycle serves to generate sulphate without O_2 , just like the modern. We argue that a contemporaneous rise of pO_2 , presumably associated with an increase in terrestrial organic carbon burial and consistent with the data presented herein (see Figure S8), drove the changes in terrestrial Fe–S cycling. Notably, this evidence for oxygenation between 420 and 387.7 Ma significantly postdates calls for a Neoproterozoic⁸ and even a putative end-Ordovician⁵⁸ increase in pO_2 and broadly agrees with recent evidence for a sustained increase in pO_2 across the Paleozoic⁵⁹. Further, the persistent preservation of anomalous sulphate throughout the Proterozoic and early Paleozoic implies that even if present, earlier oxygenation events never reached mid-Paleozoic levels of pO_2 . We find that the proliferation of vascular plants and arborescence may be the root cause of Earth's ultimate rise in pO_2 , linking evolutionary advancements preserved in fossil records to a critical transition in Earth's surface redox state. As the loss of anomalous sulphur isotope signatures has come to be the hallmark of Earth's first major oxidation⁴⁵, the loss of anomalous oxygen isotope signatures may mark the second and final rise of pO_2 .

Methods

Isotope Nomenclature

Standard definitions for $\delta^{18}\text{O}$ and $\Delta^{17}\text{O}$ are as follows:

$$\delta^{18}\text{O}_{\text{sample}} = 10^3 \cdot \left(\frac{{}^{18}\text{R}_{\text{sample}}}{{}^{18}\text{R}_{\text{standard}}} - 1 \right) \quad (1)$$

and

$$\Delta^{17}\text{O}_{\text{sample}} = 10^3 \cdot \left(\ln \left(\frac{\delta^{17}\text{O}_{\text{sample}}}{1000} + 1 \right) - \theta_{\text{RF}} \cdot \ln \left(\frac{\delta^{18}\text{O}_{\text{sample}}}{1000} + 1 \right) \right) \quad (2)$$

Here, θ_{RF} is the slope of the mass dependent reference line, which we define as $\theta_{\text{RF}} = 0.5305$. Using a set of internal standards, we report a precision on sulfate of $\pm 0.02\text{‰}$ (1σ) for $\Delta^{17}\text{O}$. All $\delta^{18}\text{O}$ values are reported with respect to VSMOW using a scale and drift correction using IAEA-SO5 and IAEA-SO6. The $\Delta^{17}\text{O}$ data is presented on the silicate-derived VSMOW/SLAP scale described below.

Sample Treatment

There are four main stages in the preparation and analysis of the $\Delta^{17}\text{O}$ of natural sulphate samples: (1) chemical purification, (2) conversion to analyte gas using a fluorinating agent, (3) analyte gas purification protocols, and (4) data treatment and standardization. (1) Two methods were used to purify sulphate in this study: a) ion exchange resin chromatography⁶⁰ and b) dissolution in a chelating solution of diethylenetriamine pentaacetate (DTPA)⁶¹. Both methods precipitate BaSO_4 from purified SO_4^{2-} solutions and yield isotopically indistinguishable results. (2) BaSO_4 conversion to analyte O_2 was performed by laser heating under an F_2 atmosphere^{37,62}. This method

results in non-quantitative O_2 yields. Yields at Harvard University are on average $33 \pm 8\%$ (full range from 11–58%) for F_2 fluorination and sample gas cleaning and are reported with all published data such that data can be corrected. (3) Analyte O_2 gas was purified via a series of cryogenic and chromatographic steps prior to isotopic analysis³⁷. We ensured that nitrogen-containing compounds were removed prior to analysis, to prevent isobaric interferences with the ^{17}O -containing m/z 33 beam⁶³. (4) All data here (standards and unknowns) are reported on a VSMOW/SLAP scale using a three-point silicate-air reference frame (UWG-2: $\delta^{18}\text{O} = 5.70\text{‰}$, $\Delta^{17}\text{O} = -0.085\text{‰}$; NBS 28: $\delta^{18}\text{O} = 9.58\text{‰}$, $\Delta^{17}\text{O} = -0.083\text{‰}$; air O_2 : $\delta^{18}\text{O} = 24.05\text{‰}$, $\Delta^{17}\text{O} = -0.501\text{‰}$) with accepted values⁶⁴.

Inter-Lab and Inter-Method Data Comparison

Data in this study and from previous work^{16,18,19,24} has been scaled for direct comparison. Due to isobaric interferences, the measurement of a triple-oxygen isotope composition in sulphate is performed by converting SO_4^{2-} to O_2 , the measured analyte gas. Several methods exist to achieve this conversion (e.g.^{37,65,66}), and these are not uniform between labs and datasets, nor are published standardizations. Methods such as laser fluorination (used in this study) that do not generate 100% yield of SO_4^{2-} – O inherently introduce greater uncertainty. It is important to note that as new labs and new methods^{65,66} become available, rigorous inter-lab and inter-method comparisons are being undertaken⁶⁶.

Data availability

The sulphate triple oxygen isotope data generated in this study are provided in the Supplementary Information.

References

- Hayes, J. M. & Waldbauer, J. R. The carbon cycle and associated redox processes through time. *Philos. Trans. R. Soc. B: Biol. Sci.* **361**, 931–950 (2006).
- Garrels, R. M. & Lerman, A. Phanerozoic cycles of sedimentary carbon and sulfur. *Proc. Natl Acad. Sci.* **78**, 4652–4656 (1981).
- Bergman, N. M., Lenton, T. M. & Watson, A. J. COPSE: a new model of biogeochemical cycling over Phanerozoic time. *Am. J. Sci.* **304**, 397–437 (2004).
- Berner, R. A., Beerling, D. J., Dudley, R., Robinson, J. M. & Wildman, R. A. Jr Phanerozoic atmospheric oxygen. *Annu. Rev. Earth Planet. Sci.* **31**, 105–134 (2003).
- Scott, C. et al. Tracing the stepwise oxygenation of the Proterozoic ocean. *Nature* **452**, 456–459 (2008).
- Sperling, E. A. et al. Statistical analysis of iron geochemical data suggests limited late Proterozoic oxygenation. *Nature* **523**, 451–454 (2015).
- Sperling, E. A. et al. A long-term record of early to mid-Paleozoic marine redox change. *Sci. Adv.* **7**, eabf4382 (2021).
- Och, L. M. & Shields-Zhou, G. A. The Neoproterozoic oxygenation event: Environmental perturbations and biogeochemical cycling. *Earth-Sci. Rev.* **110**, 26–57 (2012).
- Planavsky, N. J. et al. Low Mid-Proterozoic atmospheric oxygen levels and the delayed rise of animals. *Science* **346**, 635–638 (2014).
- Sperling, E. A., Knoll, A. H. & Girguis, P. R. The ecological physiology of Earth's second oxygen revolution. *Annu. Rev. Ecol., Evolution, Syst.* **46**, 215–235 (2015).
- Sahoo, S. K. et al. Oceanic oxygenation events in the anoxic Ediacaran ocean. *Geobiology* **14**, 457–468 (2016).
- Lu, W. et al. Late inception of a resiliently oxygenated upper ocean. *Science* **361**, 174–177 (2018).
- Warke, M. R. et al. The Great Oxidation Event preceded a Paleoproterozoic "snowball Earth". *Proc. Natl Acad. Sci.* **117**, 13314–13320 (2020).

14. Crockford, P. W. et al. Triple oxygen isotope evidence for limited mid-Proterozoic primary productivity. *Nature* **559**, 613–616 (2018).
15. Thiemens, M. H. History and applications of mass-independent isotope effects. *Annu. Rev. Earth Planet. Sci.* **34**, 217–262 (2006).
16. Bao, H., Lyons, J. R. & Zhou, C. Triple oxygen isotope evidence for elevated CO₂ levels after a Neoproterozoic glaciation. *Nature* **453**, 504–506 (2008).
17. Hodgskiss, M. S., Crockford, P. W., Peng, Y., Wing, B. A. & Horner, T. J. A productivity collapse to end Earth's Great Oxidation. *Proc. Natl Acad. Sci.* **116**, 17207–17212 (2019).
18. Crockford, P. W. et al. Claypool continued: Extending the isotopic record of sedimentary sulfate. *Chem. Geol.* **513**, 200–225 (2019).
19. Waldeck, A. R., Hemingway, J. D., Yao, W., Paytan, A. & Johnston, D. T. The triple oxygen isotope composition of marine sulfate and 130 million years of microbial control. *Proc. Natl Acad. Sci.* **119**, e2202018119 (2022).
20. Waldeck, A. R. et al. Deciphering the atmospheric signal in marine sulfate oxygen isotope composition. *Earth Planet. Sci. Lett.* **522**, 12–19 (2019).
21. Killingsworth, B. A., Bao, H. & Kohl, I. E. Assessing pyrite-derived sulfate in the Mississippi River with four years of sulfur and triple-oxygen isotope data. *Environ. Sci. Technol.* **52**, 6126–6136 (2018).
22. Hemingway, J. D. et al. Triple oxygen isotope insight into terrestrial pyrite oxidation. *Proc. Natl Acad. Sci.* **117**, 7650–7657 (2020).
23. Hemingway, J. D., Goldberg, M. L., Sutherland, K. M. & Johnston, D. T. Theoretical estimates of sulfoxyanion triple-oxygen equilibrium isotope effects and their implications. *Geochimica et. Cosmochimica Acta* **336**, 353–371 (2022).
24. Waldeck, A. R. et al. Calibrating the triple oxygen isotope composition of evaporite minerals as a proxy for marine sulfate. *Earth Planet. Sci. Lett.* **578**, 117320 (2022).
25. Bertran, E. et al. Oxygen isotope effects during microbial sulfate reduction: applications to sediment cell abundances. *ISME J.* **14**, 1508–1519 (2020).
26. Moses, C. O., Nordstrom, D. K., Herman, J. S. & Mills, A. L. Aqueous pyrite oxidation by dissolved oxygen and by ferric iron. *Geochimica et. Cosmochimica Acta* **51**, 1561–1571 (1987).
27. Rimstidt, J. D. & Vaughan, D. J. Pyrite oxidation: a state-of-the-art assessment of the reaction mechanism. *Geochimica et. Cosmochimica Acta* **67**, 873–880 (2003).
28. Gu, X., Heaney, P. J., Reis, F. D. A. & Brantley, S. L. Deep abiotic weathering of pyrite. *Science* **370**, eabb8092 (2020).
29. Taylor, B. E., Wheeler, M. C. & Nordstrom, D. K. Stable isotope geochemistry of acid mine drainage: Experimental oxidation of pyrite. *Geochimica et. Cosmochimica Acta* **48**, 2669–2678 (1984).
30. Reedy, B. J., Beattie, J. K. & Lowson, R. T. A vibrational spectroscopic ¹⁸O tracer study of pyrite oxidation. *Geochimica et. Cosmochimica Acta* **55**, 1609–1614 (1991).
31. Van Stempvoort, D. R., & Krouse, H. R. (1994). Controls of $\delta^{18}\text{O}$ in sulfate: Review of experimental data and application to specific environments.
32. Balci, N., Shanks, W. C. III, Mayer, B. & Mandernack, K. W. Oxygen and sulfur isotope systematics of sulfate produced by bacterial and abiotic oxidation of pyrite. *Geochimica et. Cosmochimica Acta* **71**, 3796–3811 (2007).
33. Heidel, C., Tichomirowa, M. & Junghans, M. The influence of pyrite grain size on the final oxygen isotope difference between sulphate and water in aerobic pyrite oxidation experiments. *Isotopes Environ. Health Stud.* **45**, 321–342 (2009).
34. Tichomirowa, M. & Junghans, M. Oxygen isotope evidence for sorption of molecular oxygen to pyrite surface sites and incorporation into sulfate in oxidation experiments. *Appl. Geochem.* **24**, 2072–2092 (2009).
35. Heidel, C. & Tichomirowa, M. The role of dissolved molecular oxygen in abiotic pyrite oxidation under acid pH conditions—experiments with ¹⁸O-enriched molecular oxygen. *Appl. Geochem.* **25**, 1664–1675 (2010).
36. Kohl, I. & Bao, H. Triple-oxygen-isotope determination of molecular oxygen incorporation in sulfate produced during abiotic pyrite oxidation (pH= 2–11). *Geochimica et. Cosmochimica Acta* **75**, 1785–1798 (2011).
37. Cowie, B. R. & Johnston, D. T. High-precision measurement and standard calibration of triple oxygen isotopic compositions ($\delta^{18}\text{O}$, $\Delta' 17\text{O}$) of sulfate by F₂ laser fluorination. *Chem. Geol.* **440**, 50–59 (2016).
38. Bao, H., Fairchild, I. J., Wynn, P. M. & Spötl, C. Stretching the envelope of past surface environments: Neoproterozoic glacial lakes from Svalbard. *Science* **323**, 119–122 (2009).
39. Lyons, T. W., Reinhard, C. T. & Planavsky, N. J. The rise of oxygen in Earth's early ocean and atmosphere. *Nature* **506**, 307–315 (2014).
40. Canfield, D. E. & Farquhar, J. Animal evolution, bioturbation, and the sulfate concentration of the oceans. *Proc. Natl Acad. Sci.* **106**, 8123–8127 (2009).
41. Tarhan, L. G., Droser, M. L., Planavsky, N. J. & Johnston, D. T. Protracted development of bioturbation through the early Palaeozoic Era. *Nat. Geosci.* **8**, 865–869 (2015).
42. Jackson, G. D., Iannelli, T. R., Knight, R. D., & Lebel, D. Neohelikian Bylot Supergroup of Borden Rift Basin, northwestern Baffin Island, District of Franklin. *Current research, part A. Geological Survey of Canada, Paper*, 639–649 (1985).
43. Retallack, G. J. Early forest soils and their role in Devonian global change. *Science* **276**, 583–585 (1997).
44. Dahl, T. W. & Arens, S. K. The impacts of land plant evolution on Earth's climate and oxygenation state—An interdisciplinary review. *Chem. Geol.* **547**, 119665 (2020).
45. Farquhar, J., Bao, H. & Thiemens, M. Atmospheric influence of Earth's earliest sulfur cycle. *Science* **289**, 756–758 (2000).
46. Poulton, S. W. et al. A 200-million-year delay in permanent atmospheric oxygenation. *Nature* **592**, 232–236 (2021).
47. Liu, P. et al. Triple oxygen isotope constraints on atmospheric O₂ and biological productivity during the mid-Proterozoic. *Proc. Natl Acad. Sci. USA* **118**, e2105074118 (2021).
48. Leavitt, W. D., Halevy, I., Bradley, A. S. & Johnston, D. T. Influence of sulfate reduction rates on the Phanerozoic sulfur isotope record. *Proc. Natl Acad. Sci. USA* **110**, 11244–11249 (2013).
49. Maffre, P. et al. The complex response of continental silicate rock weathering to the colonization of the continents by vascular plants in the Devonian. *Am. J. Sci.* **322**, 461–492 (2022).
50. McMahon, W. J. & Davies, N. S. Evolution of alluvial mudrock forced by early land plants. *Science* **359**, 1022–1024 (2018).
51. Kalderon-Asael, B. et al. A lithium-isotope perspective on the evolution of carbon and silicon cycles. *Nature* **595**, 394–398 (2021).
52. Müller, I. A., Brunner, B. & Coleman, M. Isotopic evidence of the pivotal role of sulfite oxidation in shaping the oxygen isotope signature of sulfate. *Chem. Geol.* **354**, 186–202 (2013).
53. Berner, R. A. GEOCARBSULF: a combined model for Phanerozoic atmospheric O₂ and CO₂. *Geochimica et. Cosmochimica Acta* **70**, 5653–5664 (2006).
54. Lenton, T. M., Daines, S. J. & Mills, B. J. COPSE reloaded: an improved model of biogeochemical cycling over Phanerozoic time. *Earth-Sci. Rev.* **178**, 1–28 (2018).
55. Elick, J. M., Driese, S. G. & Mora, C. I. Very large plant and root traces from the Early to Middle Devonian: implications for early terrestrial ecosystems and atmospheric p (CO₂). *Geology* **26**, 143–146 (1998).
56. Berkner, L. V. & Marshall, L. C. On the origin and rise of oxygen concentration in the Earth's atmosphere. *J. Atmos. Sci.* **22**, 225–261 (1965).
57. Lenton, T. M. et al. Earliest land plants created modern levels of atmospheric oxygen. *Proc. Natl Acad. Sci.* **113**, 9704–9709 (2016).

58. Edwards, C. T., Saltzman, M. R., Royer, D. L. & Fike, D. A. Oxygenation as a driver of the Great Ordovician Biodiversification Event. *Nat. Geosci.* **10**, 925–929 (2017).
59. Stockey, R. G. et al. Sustained increases in atmospheric oxygen and marine productivity in the Neoproterozoic and Palaeozoic eras. *Nat. Geosci.* **17**, 667–674 (2024).
60. Le Gendre, E., Martin, E., Villemant, B., Cartigny, P. & Assayag, N. A simple and reliable anion-exchange resin method for sulfate extraction and purification suitable for multiple O-and S-isotope measurements. *Rapid Commun. Mass Spectrom.* **31**, 137–144 (2017).
61. Bao, H. Purifying barite for oxygen isotope measurement by dissolution and reprecipitation in a chelating solution. *Anal. Chem.* **78**, 304–309 (2006).
62. Bao, H. et al. Anomalous ^{17}O compositions in massive sulphate deposits on the Earth. *Nature* **406**, 176–178 (2000).
63. Yeung, L. Y., Hayles, J. A., Hu, H., Ash, J. L. & Sun, T. Scale distortion from pressure baselines as a source of inaccuracy in triple-isotope measurements. *Rapid Commun. Mass Spectrom.* **32**, 1811–1821 (2018).
64. Wostbrock, J. A., Cano, E. J. & Sharp, Z. D. An internally consistent triple oxygen isotope calibration of standards for silicates, carbonates and air relative to VSMOW2 and SLAP2. *Chem. Geol.* **533**, 119432 (2020).
65. Ellis, N. M. & Passey, B. H. A novel method for high-precision triple oxygen isotope analysis of diverse Earth materials using high temperature conversion–methanation–fluorination and isotope ratio mass spectrometry. *Chem. Geol.* **635**, 121616 (2023).
66. Wei, Y., Yan, H., Peng, Y. & Bao, H. Quantitative Conversion of Sulfate Oxygen for High-Precision Triple Oxygen Isotope Analysis. *Anal. Chem.* **96**, 19387–19395 (2024).

Acknowledgements

We thank Julien Foriel, Jordon Hemingway, Eleanor Hughes, and Hanon McShea for lab assistance and helpful discussions. Clara Blätler, John Higgins, and Judy Pu shared samples that made this work possible. This research used samples and data provided by the International Ocean Discovery Program (IODP), United States Geological Survey (USGS) Core Repository, Canadian Geological Survey, and the Iowa Geological Survey's Oakdale Rock Library. We thank the Ministry of Energy and Minerals of the Sultanate of Oman and Petroleum Development Oman (PDO) for permission to publish results from subsurface evaporite samples. We thank Irene Gómez-Pérez and Aisha Al-Hajri at PDO and Shuram LLC for providing assistance with the PDO core repository. A.R.W., H.C.O., and D.T.J. were supported by NSF OCE-1946137, awarded to D.T.J.

Author contributions

A.R.W., H.C.O., B.R.C., F.A.M., and D.T.J. designed the research. A.R.W., E.B.H., K.D.B., K.D., S.E.G., and R.J.C. provided samples. A.R.W., H.C.O., B.R.C., A.M.C., and D.T.J. performed analyses. A.R.W., H.C.O., P.W.C., A.M.C., B.R.C., E.B.H., K.D.B., K.D., S.E.G., R.J.C., F.A.M., and D.T.J. contributed to data analysis and the writing of the manuscript.

Competing interests

The authors declare no competing interests.

Additional information

Supplementary information The online version contains supplementary material available at <https://doi.org/10.1038/s41467-025-57282-y>.

Correspondence and requests for materials should be addressed to Anna R. Waldeck, Haley C. Olson or David T. Johnston.

Peer review information *Nature Communications* thanks Benjamin W Johnson, Wenkun Qie and Haiyang Wang for their contribution to the peer review of this work. A peer review file is available.

Reprints and permissions information is available at <http://www.nature.com/reprints>

Publisher's note Springer Nature remains neutral with regard to jurisdictional claims in published maps and institutional affiliations.

Open Access This article is licensed under a Creative Commons Attribution-NonCommercial-NoDerivatives 4.0 International License, which permits any non-commercial use, sharing, distribution and reproduction in any medium or format, as long as you give appropriate credit to the original author(s) and the source, provide a link to the Creative Commons licence, and indicate if you modified the licensed material. You do not have permission under this licence to share adapted material derived from this article or parts of it. The images or other third party material in this article are included in the article's Creative Commons licence, unless indicated otherwise in a credit line to the material. If material is not included in the article's Creative Commons licence and your intended use is not permitted by statutory regulation or exceeds the permitted use, you will need to obtain permission directly from the copyright holder. To view a copy of this licence, visit <http://creativecommons.org/licenses/by-nc-nd/4.0/>.

© The Author(s) 2025